catalysts

MDPI

Synergetic Effects of Mixed-Metal Polyoxometalates@Carbon-Based Composites as Electrocatalysts for the Oxygen Reduction and the Oxygen Evolution Reactions

Inês S. Marques[a], Bruno Jarrais[a], Israël-Martyr Mbomekallé[b], Anne-Lucie Teillout[b], Pedro de Oliveira[b], Cristina Freire[a], Diana M. Fernandes[a*]

[a] REQUIMTE/Departamento de Química e Bioquímica, Faculdade de Ciências, Universidade do Porto, 4169-007 Porto, Portugal.

[b] Institut de Chimie Physique, UMR 8000 CNRS, Université Paris-Saclay, 91405 Orsay Cedex, France.

*Corresponding authors: Dr. Diana M. Fernandes (diana.fernandes@fc.up.pt)

1. Experimental

1.1. Physicochemical characterization

X-ray photoelectron spectroscopy (XPS) measurements were performed at the Centro de Materiais da Universidade do Porto (CEMUP), Portugal, on A VG Scientific ESCALAB 200A spectrometer with non-monochromatized Al Kα radiation (1486.6 eV) was used for X-ray photoelectron spectroscopy (XPS) measurements at CEMUP. Potential deviations induced by electric charge of the samples were corrected using the C 1s band at 284.6 eV as an internal standard. The analysis of XPS results were performed using the CasaXPS software for spectra deconvolution. Surface atomic percentages were calculated from the corresponding peak areas upon spectra deconvolution and using the sensitivity factors provided by the manufacturer.

Scanning electron microscopy/Energy-dispersive X-ray spectroscopy (SEM/EDS) was carried out using a high resolution (Schottky) environmental SEM with X-ray microanalysis and electron backscattered

diffraction analysis (Quanta 400 FEG ESEM/EDAX Genesis X4M), in high-vacuum conditions, at the Centro de Materiais da Universidade do Porto (CEMUP).

1.2. Assessment of electrochemically active surface areas (ECSA)

ECSA values exhibited by electrocatalysts are usually calculated by using the equation 1:

$$ECSA = C_{dl} / C_{ref} \qquad \text{(Eq.1)}$$

where C_{dl} stands for the double-layer capacitance and C_{ref} for the reference capacitance value per unit area. Due to the impossibility of knowing the exact C_{ref} value for specific and structurally complex materials, reliable ECSA values cannot be obtained frequently. However, the linear proportional relation between ECSA and the double-layer capacitance allows performing a relative comparison for similar electrocatalysts. Taking advantage of this fact, in the present work, C_{dl} values have been directly employed as approximated ECSA estimations to assess the surface effects on the OER performances. Thus, C_{dl} values were calculated for all materials via a standard double-layer charging test, namely, the acquisition of consecutive CV plots at different scan rates (from 20 to 160 mV s^{-1}), being the double-layer capacitance estimated from the slope of a linear-fitted plot of current density at 1.15 V vs. RHE (non-faradaic region) versus the scan rate.

1.3. ORR electrochemical tests

A potentiostat/galvanostat Autolab PGSTAT 302N (ecochimie B.V., Utrecht, The Netherlands), controlled by the NOVA v2.1 software was used for the CV and LSV tests. The experiments were conducted at room temperature using a conventional three-electrode compartment cell: 1) reference electrode - Ag/AgCl (3 mol.dm^{-3} KCl, Metrohm, Utrecht, The Netherlands); 2) working electrode - glassy carbon rotating disk electrode (RDE) (3 mm of diameter, Metrohm, Utrecht, The

Netherlands); 3) auxiliary electrode - carbon rod (2 mm of diameter, Metrohm, Utrecht, The Netherlands).

Before modification, a cleaning procedure was performed to the RDE with diamond polishing pastes of 6, 3 and 1 μM (Buehler) on a microcloth pad (BAS), followed by washing with ultra-pure water (18.2 MΩ cm at 25°C, Interlab, Lisboa, Portugal). For the RRDE, the cleaning procedure was performed only with 0.3 μm alumina powder (MicroPolish Alumina, Buehler) to prevent damage of the Pt ring. The RDE was then modified through the deposition of a 5 μL drop of the selected EC dispersion onto its surface and allowing it to dry under a flux of air. The ECs dispersion was prepared as follows: 1 mg of selected material or Pt/C were mixed with isopropanol/water/Nafion solvent mixture (125/125/20 μL) and dispersed using an ultrasonic bath for at least 15 min. Electrochemical tests were carried out in N_2- or O_2-saturated KOH (0.1 mol dm^{-3}). To achieve this, the electrolyte was degassed for 30 min with the selected gas.

For the evaluation of the ORR performance, both the CV and LSV measurements were performed between E_p = 0.26 and 1.46 V vs. RHE at 0.005 V s^{-1}. Additionally, rotation speeds in the range 400 - 3000 rpm were used for the LSV experiments. For the chronoamperometry (CA) tests a rotation speed of 1600 rpm for 17h at a potential = 0.5 V vs. RHE was used.

The effective ORR current was obtained by subtracting the current obtained in N_2-saturated from that obtained in O_2-saturated electrolytes.

Even though the potential values were measured against the Ag/AgCl reference electrode, they were converted to the reversible hydrogen electrode (RHE) using the Eq. 2 for a proper comparison with the literature results.

$$E_{(RHE)} = E_{(Ag/AgCl)} + 0.059\ pH + E^{o}_{(Ag/AgCl)} \quad \text{(Eq.2)}$$

where $E_{(RHE)}$ is the potential vs. RHE, $E^{o}_{(Ag/AgCl)}$ = 0.1976 V (25 ºC) and $E_{(Ag/AgCl)}$ is the potential measured vs. Ag/AgCl.

The onset potential (E_{onset}) is defined as the potential at which the reduction of O_2 begins. According to literature, the E_{onset} can be determined by different methods and is generally assumed as the potential at which the ORR current is 5% of the diffusion-limiting current density or it can be calculated as the potential at which the slope of the voltammogram exceeds a threshold value (j = 0.1 mA $cm^{-2}V^{-1}$). Here we considered the first method.

The kinetic parameters and the number of electrons transferred per O_2 molecule (n_{O2}) in the ORR were determined using the following Koutecky-Levich (KL) equations[1]:

$$\frac{1}{j} = \frac{1}{j_L} + \frac{1}{j_k} = \frac{1}{B\omega^{1/2}} + \frac{1}{j_k} \quad \text{(Eq. 3)}$$

$$B = 0.2\ n_{O2}\ F\ (D_{O2})^{2/3}\ v^{-1/6}\ C_{O2} \quad \text{(Eq. 4)}$$

Here, j is the current density measured, j_L and j_k are the diffusion-limiting and kinetic current densities, ω is the angular velocity, F is the Faraday constant (96 485 C mol^{-1}), D_{O2} is the O_2 diffusion coefficient (1.95×10^{-5} $cm^2\ s^{-1}$), v is the electrolyte kinematic viscosity (0.008977 $cm^2\ s^{-1}$), C_{O2} is the O_2 bulk concentration (1.15×10^{-3} mol dm^{-3}). For rotation speeds in rpm is adopted a constant of 0.2[1].

Tafel plots were obtained after the measured LSV currents were corrected for diffusion to yield the corresponding kinetic current values. The j_L parameter, obtained through the combination of Eq. 3 and 4 was used to make the mass transport correction. The values of j_k obtained were normalized for the total deposited mass of EC.

Rotating ring disk electrode (RRDE) measurements in O_2-saturated KOH solution were also performed to obtain a more in-depth insight of the ORR electrocatalytic activity of the ECs. The H_2O_2 yields were determined from the ring and disk currents (i_R and i_D, respectively), and the current collection efficiency of the Pt ring (N = 0.25, in this case) using Eq. 5:

$$\% H_2O_2 = 200 \times \frac{i_R / N}{i_D + i_R / N} \quad \text{(Eq. 5)}$$

Figures

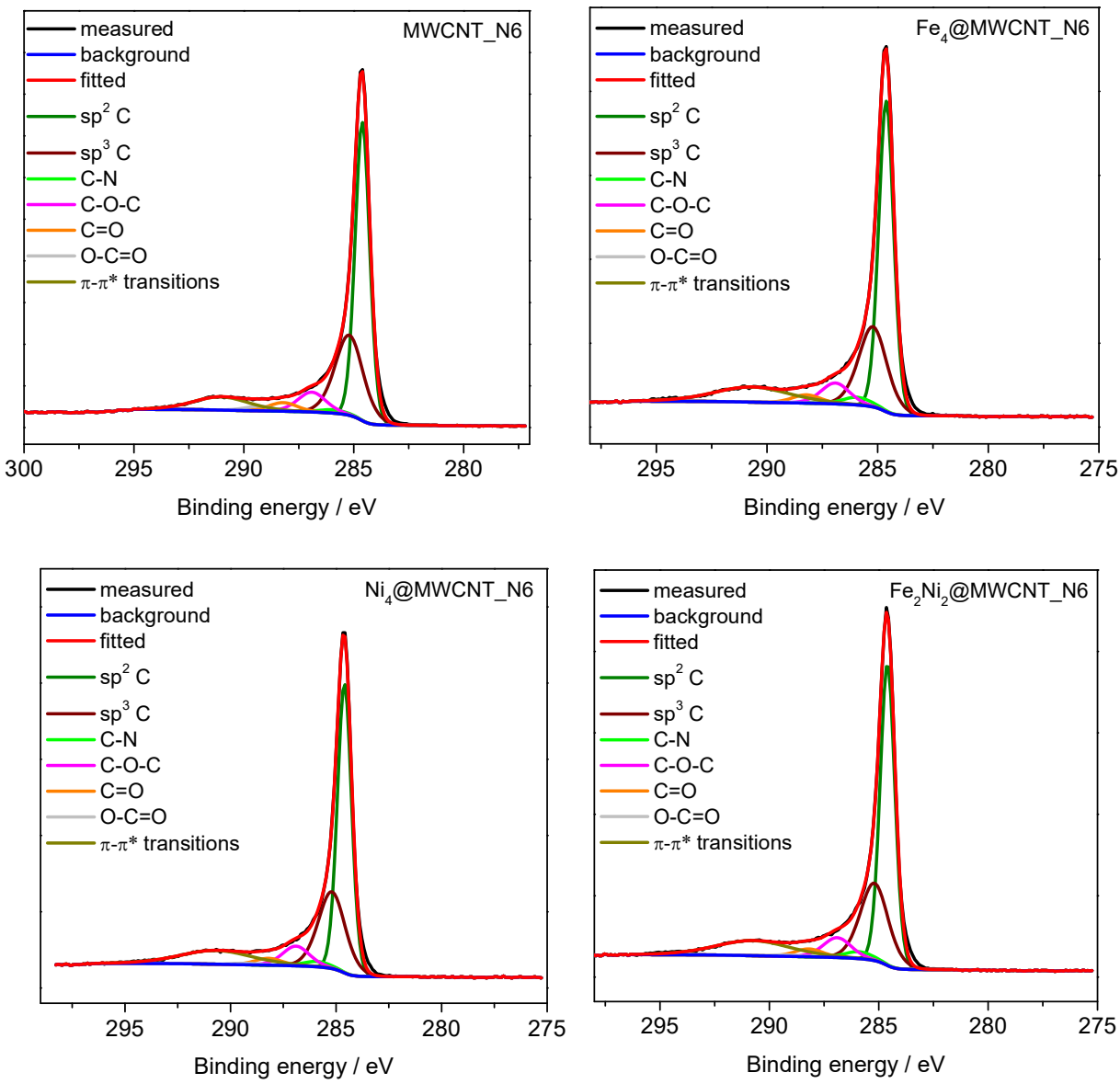

Figure S1. Deconvoluted C1s high resolution spectra of the MWCNT_N6-based materials.

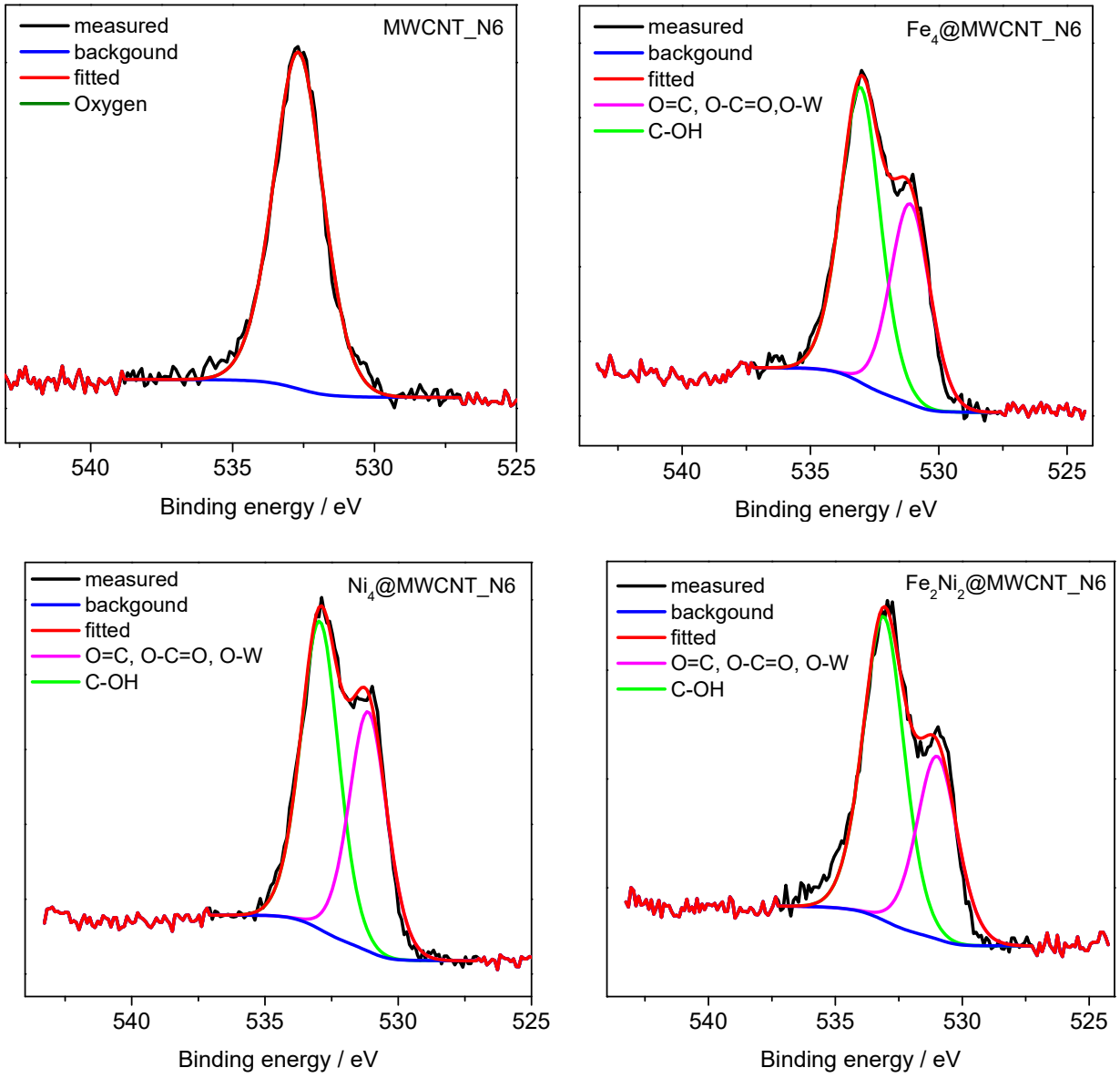

Figure S2. Deconvoluted O1s high resolution spectra of the MWCNT_N6-based materials.

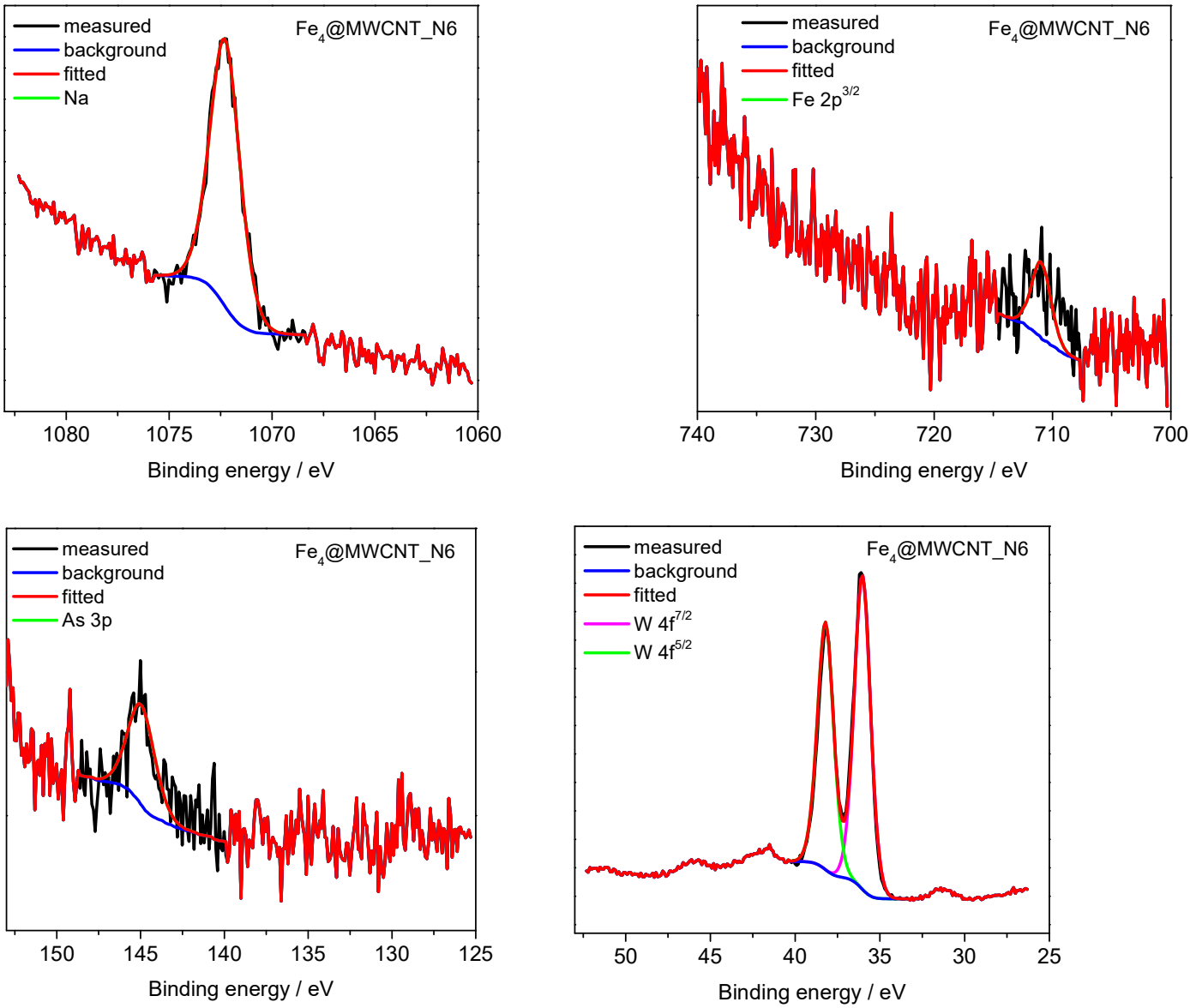

Figure S3. Deconvoluted high resolution spectra for Fe4@MWCNT_N6: Na1s (a), Fe 2p (b), As 3p (c) and W 4f (d).

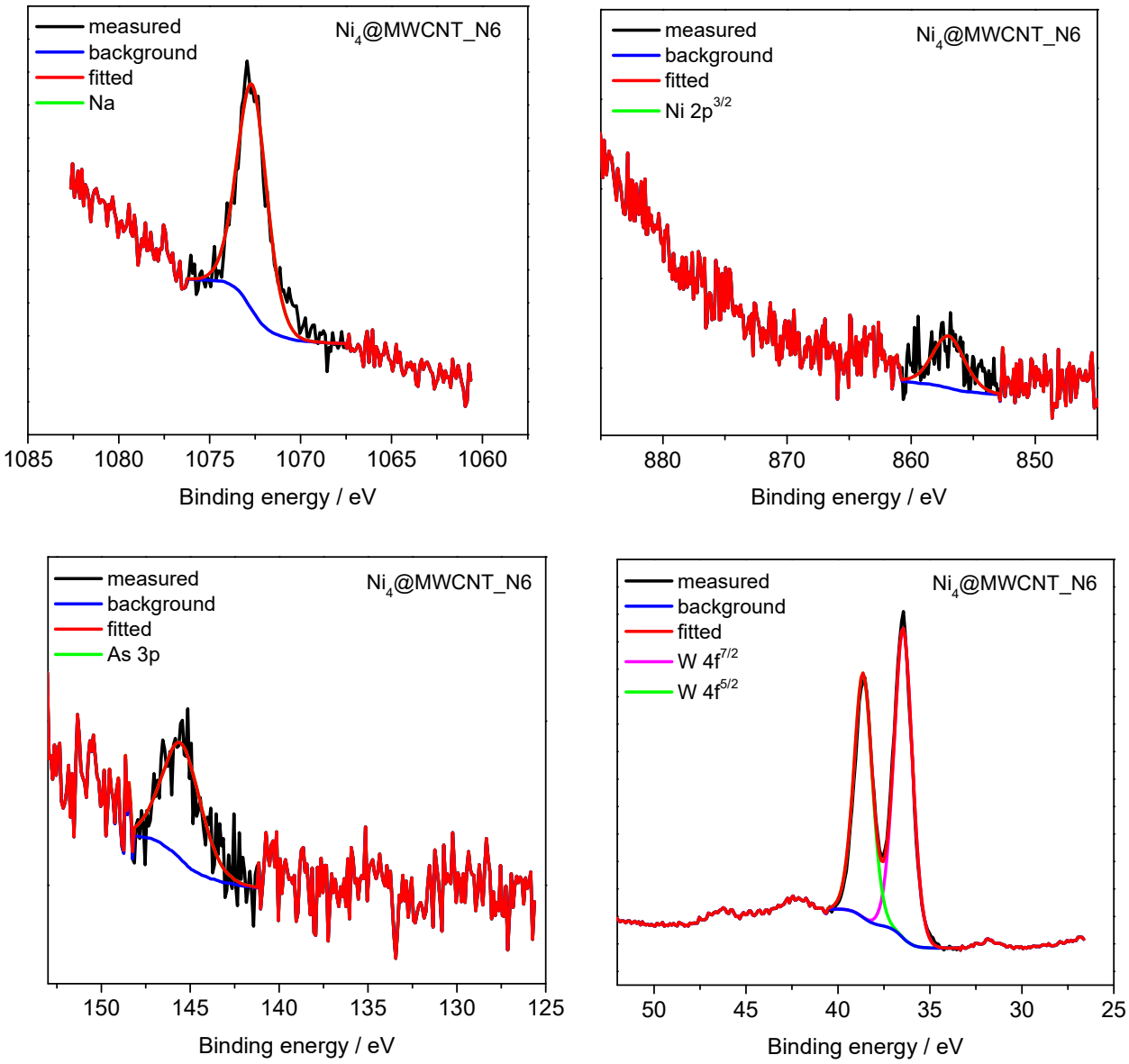

Figure S4. Deconvoluted high resolution spectra for Ni4@MWCNT_N6: Na1s (a), Ni 2p (b), As 3p (c) and W 4f (d).

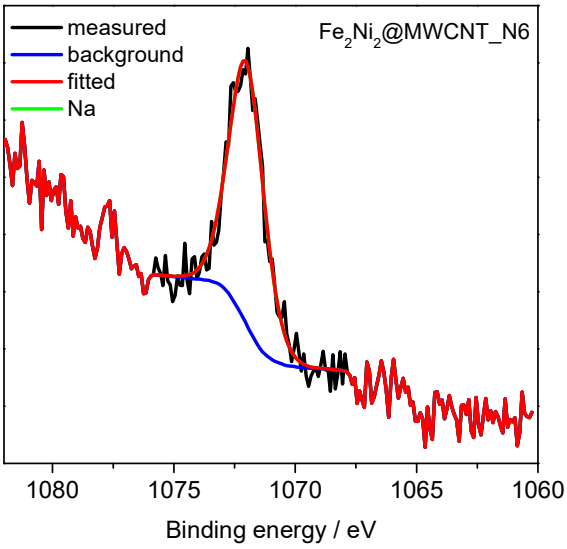
measured
background
fitted
Na
Fe2Ni2@MWCNT_N6
1080
1075
1070
1065
1060
Binding energy / eV

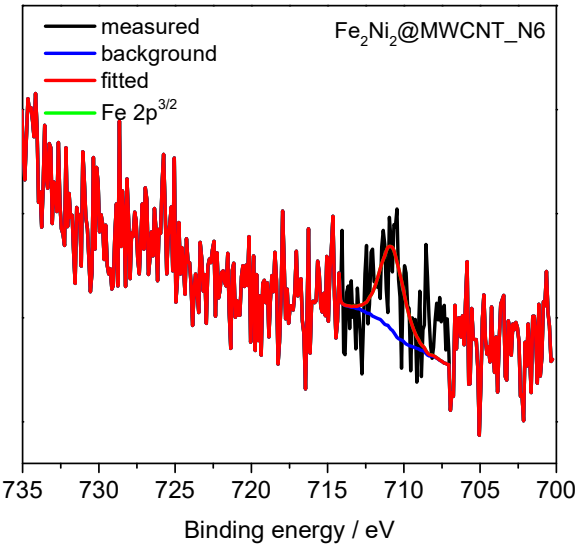
measured
background
fitted
Fe 2p3/2
Fe2Ni2@MWCNT_N6
735
730
725
720
715
710
705
700
Binding energy / eV

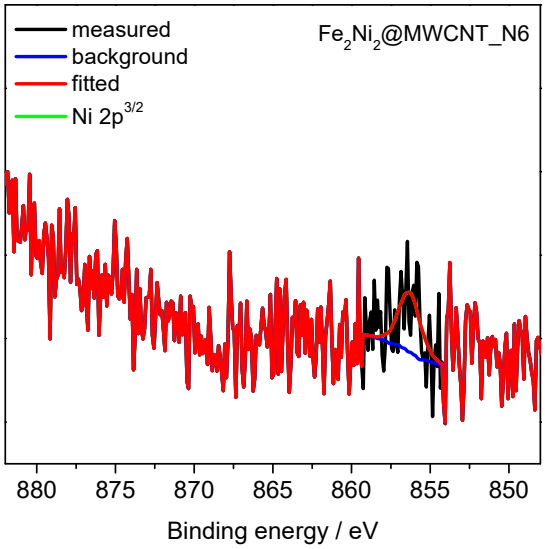
measured
background
fitted
Ni 2p3/2
Fe2Ni2@MWCNT_N6
880
875
870
865
860
855
850
Binding energy / eV

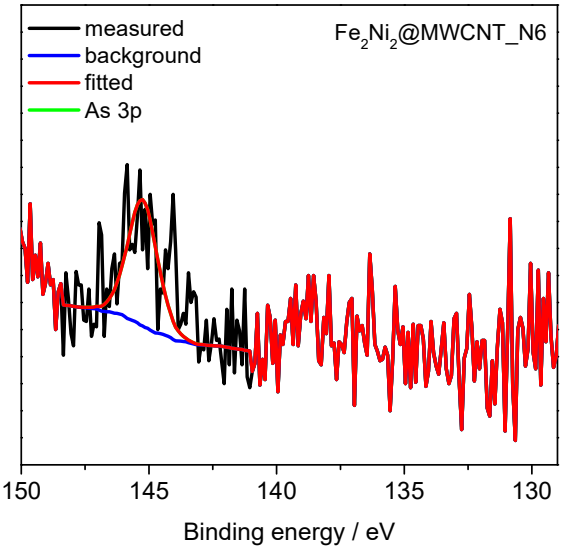
measured
background
fitted
As 3p
Fe2Ni2@MWCNT_N6
150
145
140
135
130
Binding energy / eV

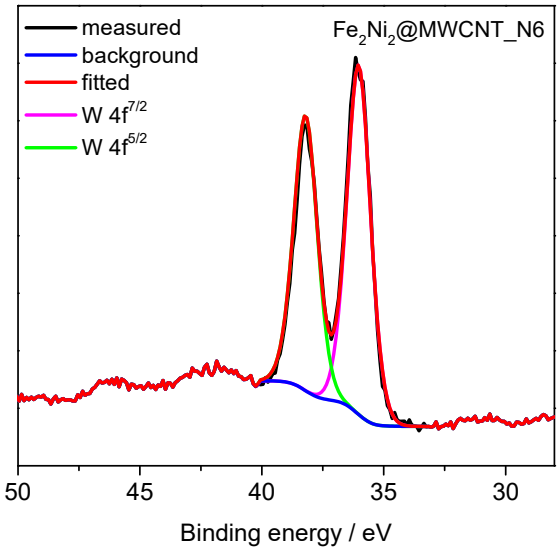

Figure S5. Deconvoluted high resolution spectra for Fe_2Ni_2@MWCNT_N6: Na1s (a), Fe 2p (b), Ni 2p (c), As 3p (d) and W 4f (e).

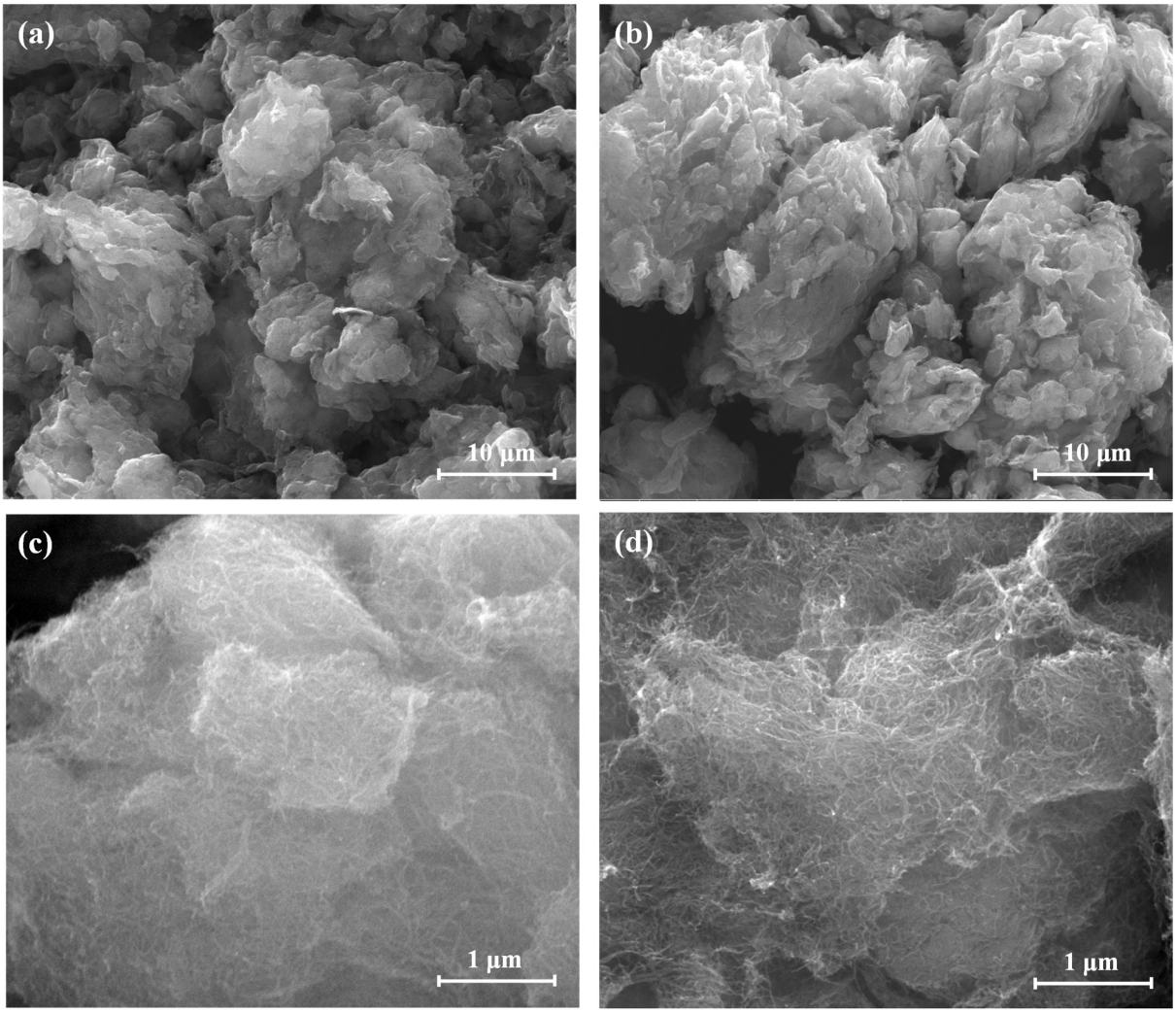

Figure S6. SEM images of Fe_4@MWCNT_N6 and Ni_4@MWCNT_N6 at ×5000 (a, b) and ×50000 (c, d) magnification.

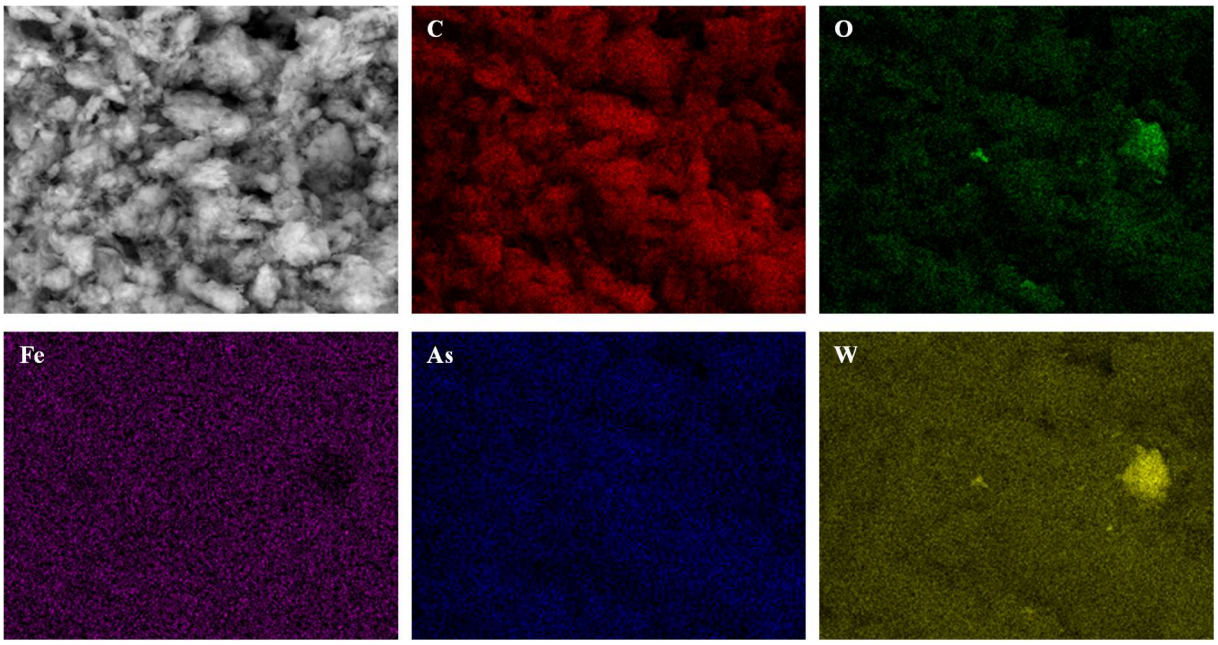

Figure S7. SEM and EDX elemental mapping images of Fe_4@MWCNT_N6 at ×2500 magnification.

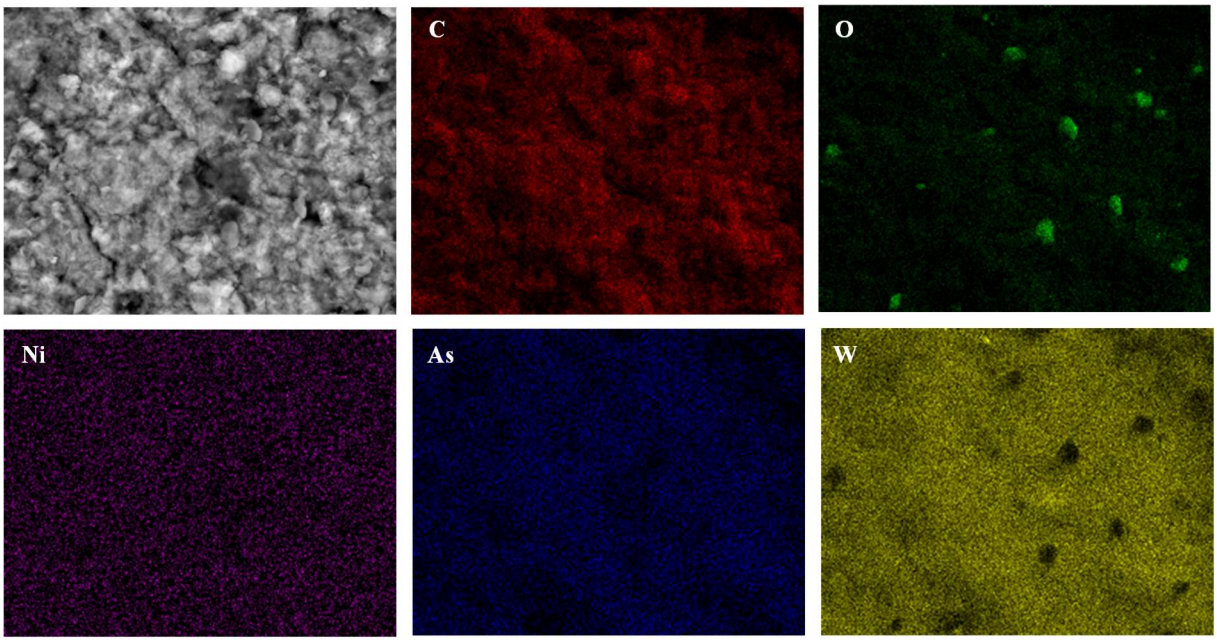

Figure S8. SEM and EDX elemental mapping images of Ni_4@MWCNT_N6 at ×2500 magnification.

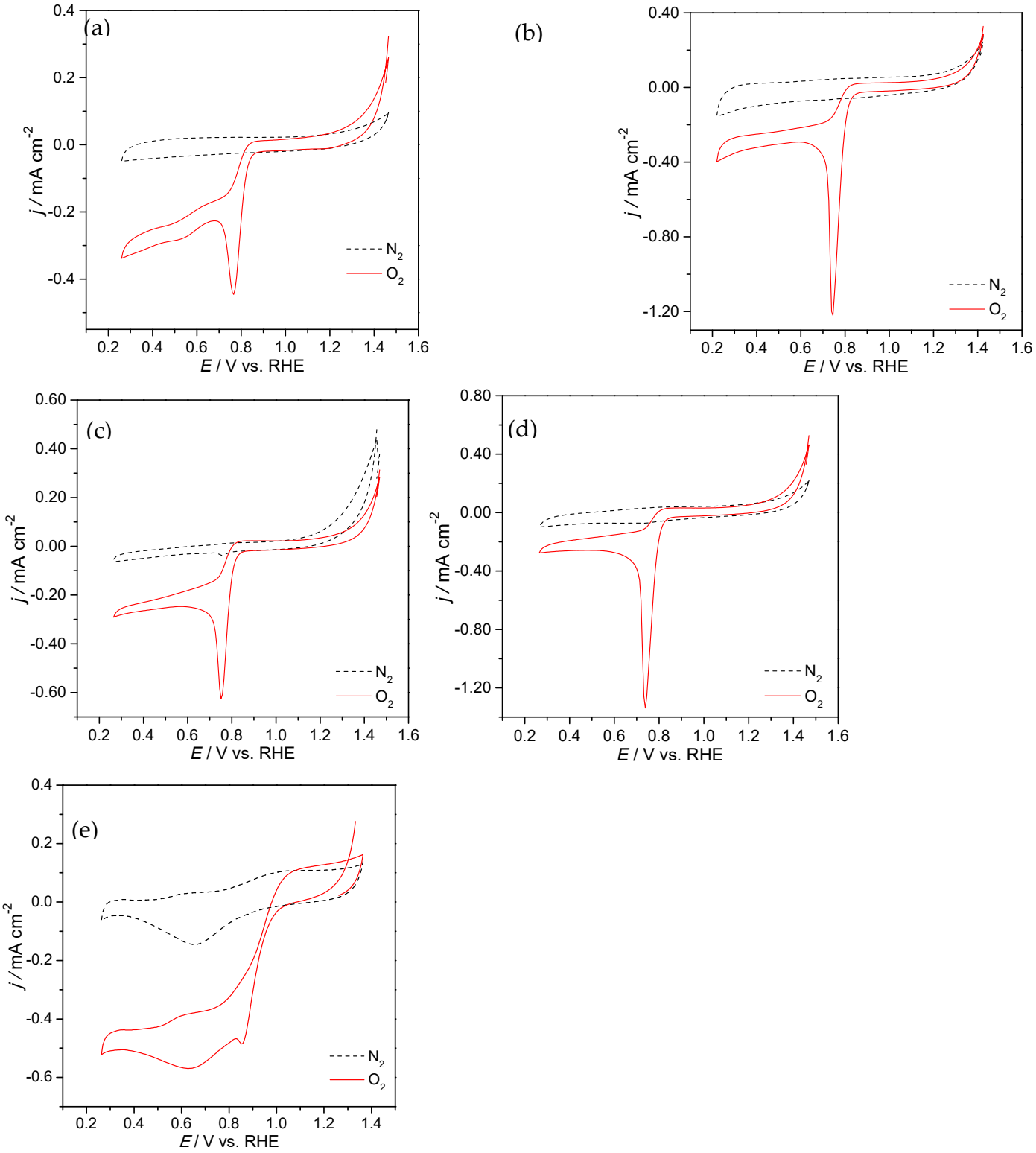

Figure S9. CVs of MWCNT_N6 (a), Fe_4@MWCNT_N6 (b), Ni_4@MWCNT_N6 (c), Fe_2Ni_2@MWCNT_N6 (d) and Pt/C (e) in N_2- (dash line) and O_2-saturated (red line) 0.1 M KOH at 5 mV s^{-1}.

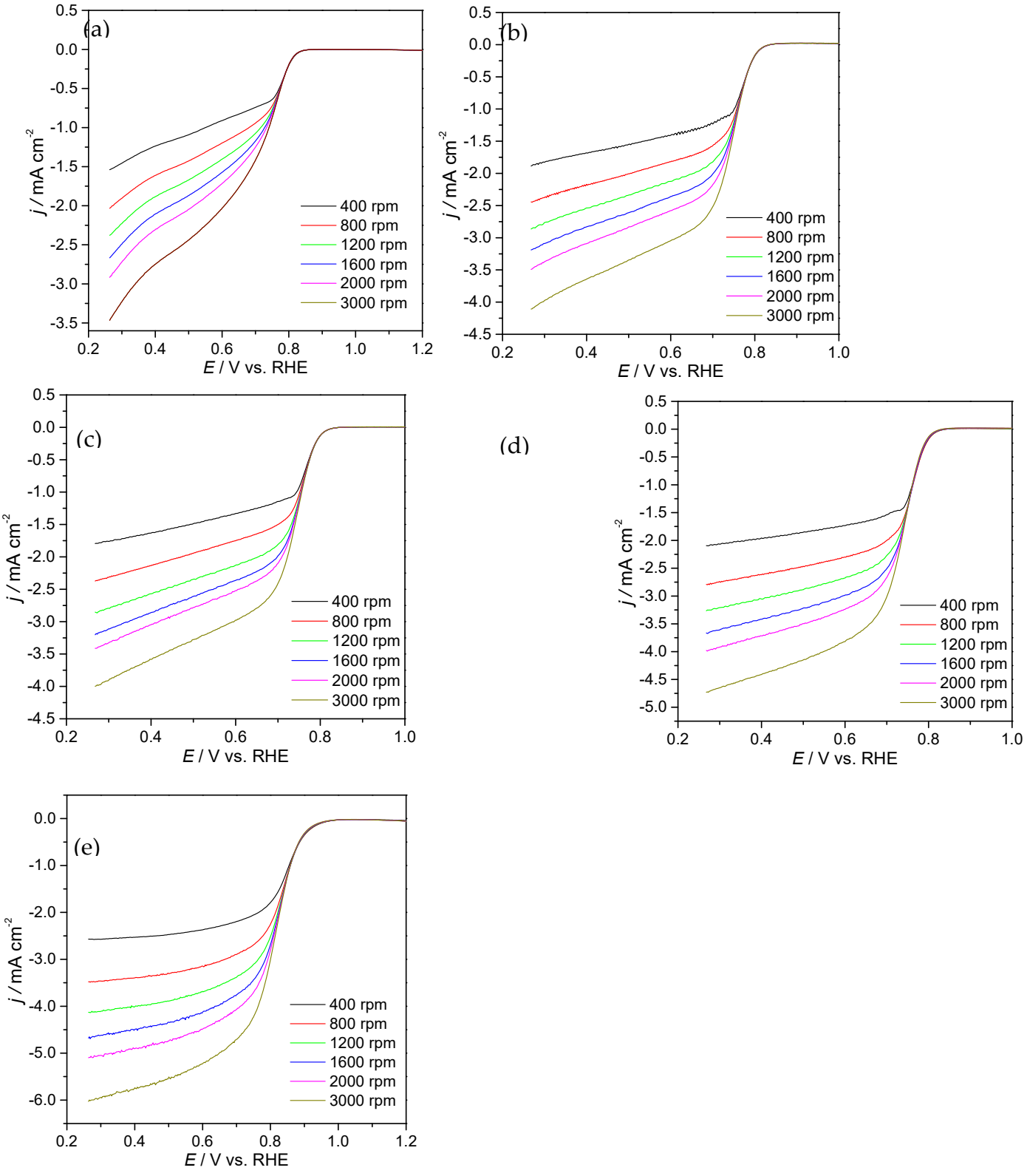

Figure S10. ORR LSVs of MWCNT_N6 (a), Fe_4@MWCNT_N6 (b), Ni_4@MWCNT_N6 (c), Fe_2Ni_2@MWCNT_N6 (d) and Pt/C (e) acquired at different rotation rates in O_2-saturated 0.1 M KOH solution at 5 mV s^{-1}.

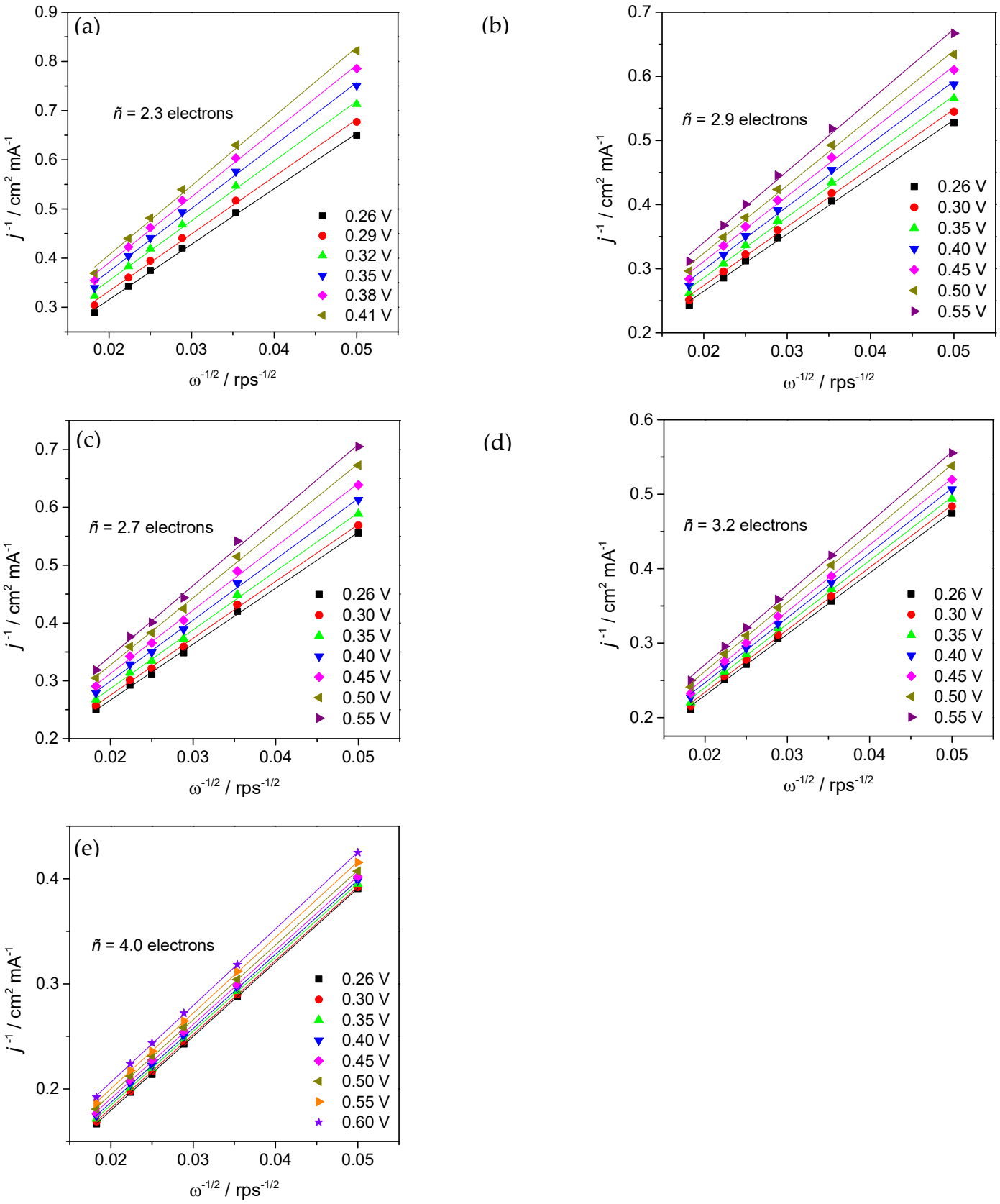

Figure S11. Koutecky-Levich (K-L) plots of MWCNT_N6 (a), Fe_4@MWCNT_N6 (b), Ni_4@MWCNT_N6 (c), Fe_2Ni_2@MWCNT_N6 (d) and Pt/C (e).

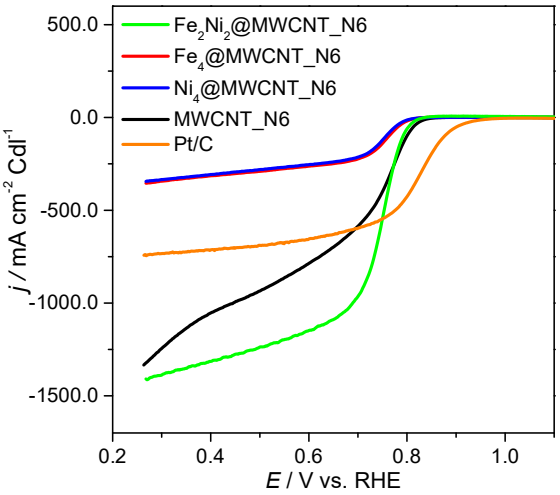

Figure S12. ORR LSV curves obtained in KOH (0.1 M) saturated with O_2 at 1600 rpm and 0.005 V s^{-1} with current densities normalized to the respective double-layer capacitance values.

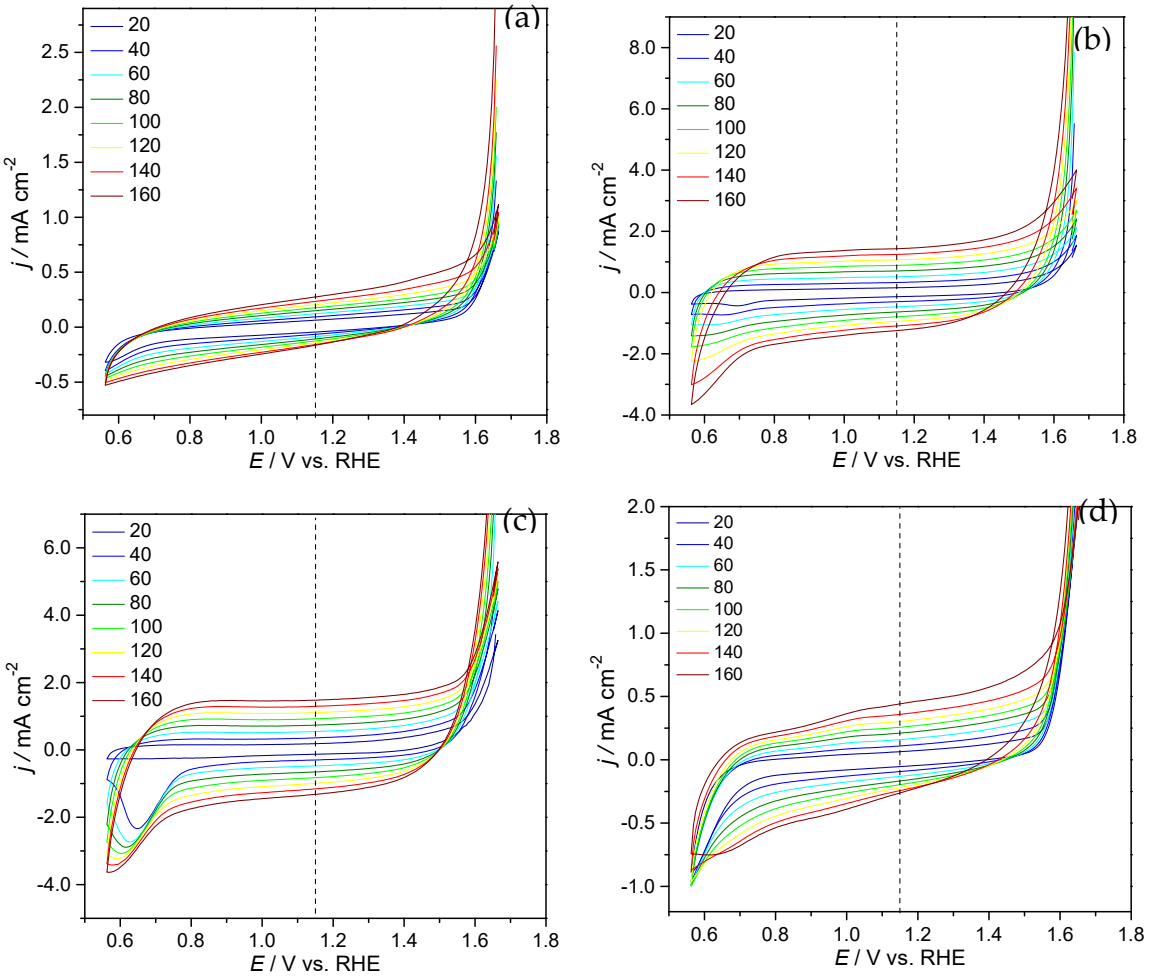

Figure S13. CVs at different scan rates for MWCNT_N6 (a), Fe_4@MWCNT_N6 (b), Ni_4@MWCNT_N6 (c), Fe_2Ni_2@MWCNT_N6 (d) in N_2-saturated KOH (0.1 M).

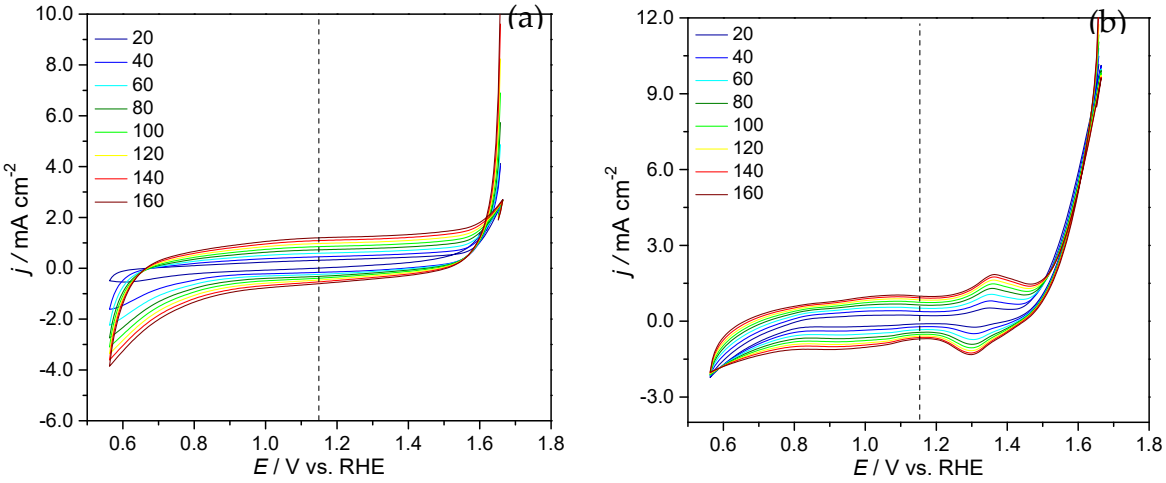

Figure S14. CVs at different scan rates of Pt/C and RuO_2 in N_2-saturated KOH (0.1 M).

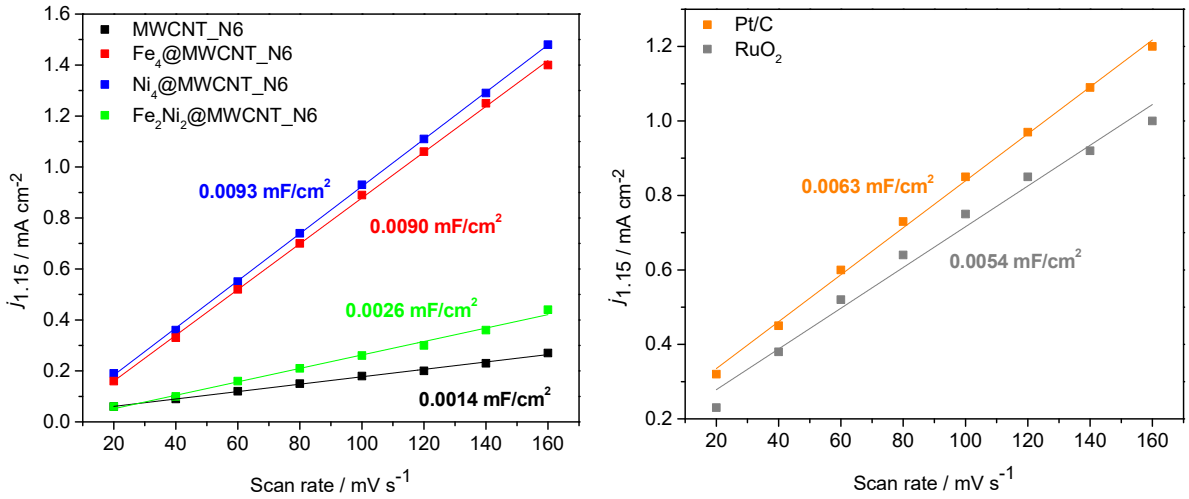

Figure S15. Current density-scan rate linear fitting plots for all materials. Numeric values correspond to the double-layer capacitances (C_{dl}) for each material.

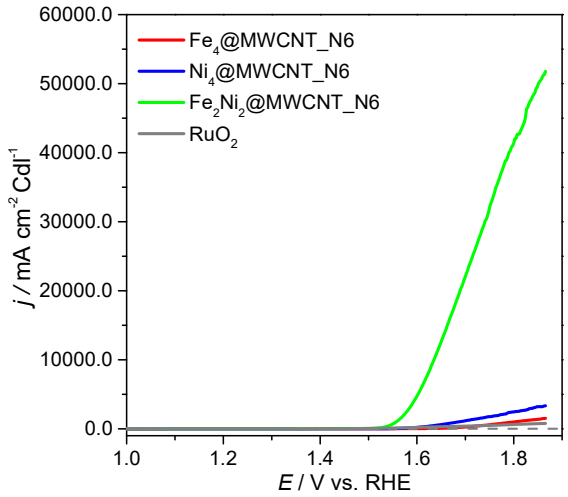

Figure S16. OER LSV curves obtained in KOH (0.1 M) saturated with N_2 at 1600 rpm and 0.005 V s^{-1} with current densities normalized to the respective double-layer capacitance values.

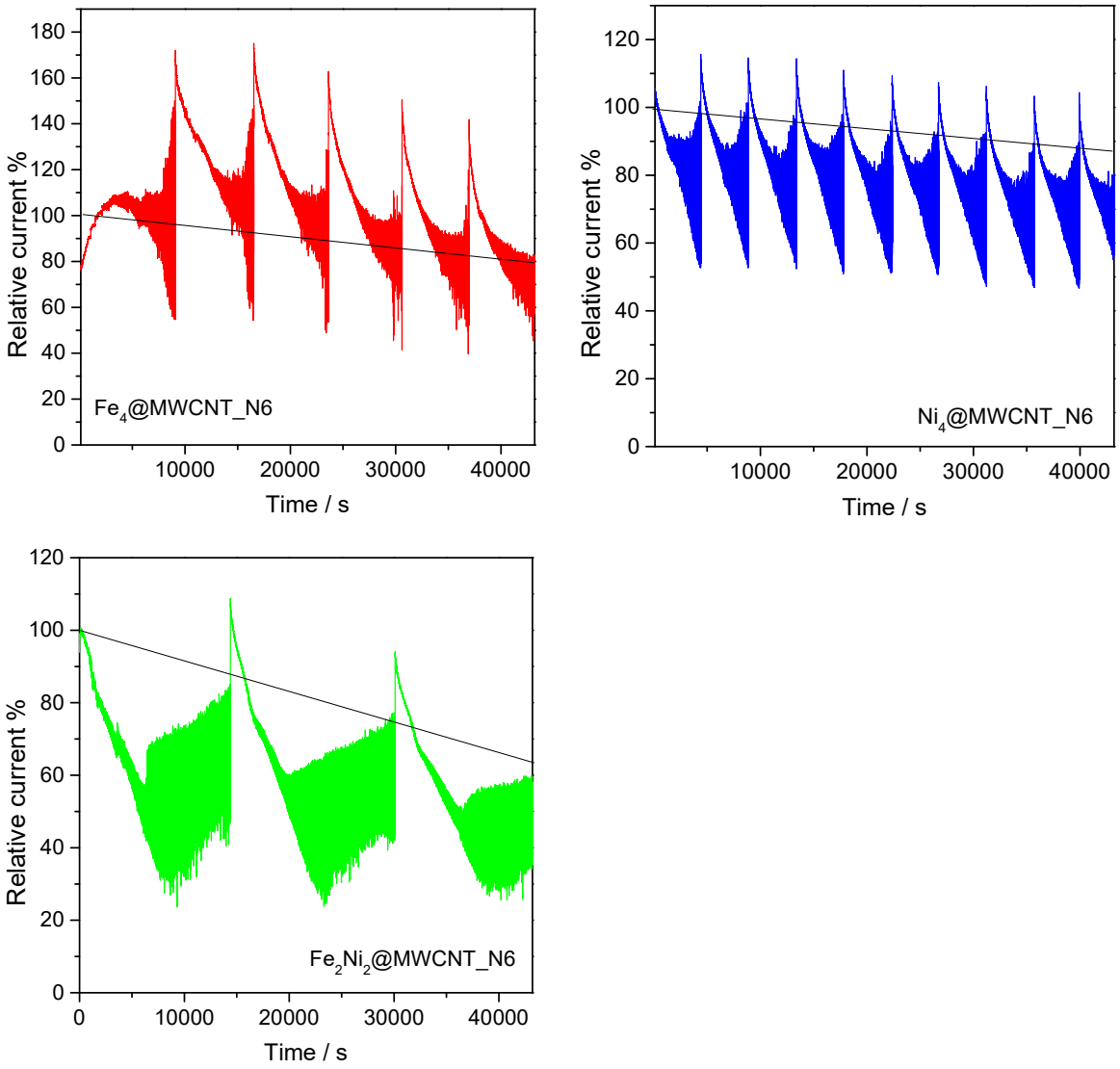

Figure S17. Chronoamperometric responses in KOH (0.1 M) saturated with N_2 at 1600 rpm for 43200 s.

Table S1. Comparison of the OER electrochemical performance (overpotentials (η_{10}), current density (j) and Tafel slopes) for similar composite materials reported in literature.

Sample	η_{10} (j=0.1mAcm^{-2})	j_{max} (mA cm^{-2})	Tafel slopes (mV dec^{-1})	Reference
Fe_4@MWCNT-N6	0.58	13.7	102	This work
Ni_4@MWCNT-N6	0.46	30.9	54	This work
Fe_2Ni_{12}@MWCNT-N6	0.36	134.6	45	This work
25@PEI@Co_4POM	0.49	33.5	60	[2]
Co_4POM/NCNT	0.37	≈6.1	203	[3]
$Co_4(PW_9)_2$@N,S-Co@C	0.41	69.9	62–124	[4]
ZIF-8@ZIF-67@PW_{12}	0.49	20	88	[5]
SiW9Co3[h]@ZIF-67	0.42	28.9	93.9	[6]
Mn/oMA-PW/RCPE	0.38	34	111	[7]
FeNi/N-C-900	0.41	32	45.3	[8]
Ni-P_{24} 3 min	0.39	35	70	[9]
Co_3O_4/$CoMoO_4$-50	0.32	-	63	[10]
20WZ-1000	0.37	-	53	[11]
FeNi@AC	0.28		388	[12]
FeNi@N-CNT	0.30	-	47.7	[13]
NiFe-NS	0.30	-	40	[14]
NiFe-Bulk	0.35	-	65	[14]
NiFe-MoO_xNS	0.28	-	55	[15]
Fe/N-CNTs	0.52	-	76	[16]
Ni/N-CNTs	0.59	-	138	[16]

NiFe/NC	0.32	-	45	[17]
NiFe-MMO/CNT	0.22	44	45	[18]

References

1. Fernandes, D.M.; Mathumba, P.; Fernandes, A.J.S.; Iwuoha, E.I.; Freire, C., Towards efficient oxygen reduction reaction electrocatalysts through graphene doping. *Electrochim. Acta* **2019**, *319*, 72–81.
2. Gong, R.H.; Gao, D.D.; Liu, R.J.; Sorsche, D.; Biskupek, J.; Kaiser, U.; Rau, S.; Streb, C., Self-Activation of a Polyoxometalate-Derived Composite Electrocatalyst for the Oxygen Evolution Reaction. *Acs Applied Energy Materials* **2021,** *4* , 12671–12676.
3. Lee, G.Y.; Kim, I.; Lim, J.; Yang, M.Y.; Choi, D.S.; Gu, Y.; Oh, Y.; Kang, S.H.; Nam, Y.S.; Kim, S.O., Spontaneous linker-free binding of polyoxometalates on nitrogen-doped carbon nanotubes for efficient water oxidation. *J. Mater. Chem. A* **2017,** *5*, 1941–1947.
4. Abdelkader-Fernandez, V.K.; Fernandes, D.M.; Cunha-Silva, L.; Fernandes, A.J.S.; Freire, C., Decorating MOF-74-derived nanocarbons with a sandwich-type polyoxometalate to enhance their OER activity: Exploring the underestimated bulk-deposition approach. *Electrochim. Acta* **2021,** *389*.
5. Wang, Y.; Wang, Y.Y.; Zhang, L.; Liu, C.S.; Pang, H., Core-shell-type ZIF-8@ZIF-67@POM hybrids as efficient electrocatalysts for the oxygen evolution reaction. *Inorg. Chem. Front.* **2019,** *6*, 2514–2520.
6. Abdelkader-Fernandez, V.K.; Fernandes, D.M.; Balula, S.S.; Cunha-Silva, L.; Freire, C., Advanced framework-modified POM@ZIF-67 nanocomposites as enhanced oxygen evolution reaction electrocatalysts. *J. Mater. Chem. A* **2020,** *8*, 13509–13521.
7. Imani, A.H.; Ojani, R.; Raoof, J.B., Novel polyoxometalate-based composite as efficient electrocatalyst for alkaline water oxidation reaction. *Journal of the Iranian Chemical Society* **2021,** *18*, 2079–2089.
8. Zhang, C.X.; Wu, C.; Gao, Y.; Gong, Y.; Liu, H.Y.; He, J.P., FeNi Nanoparticles Coated on N-doped Ultrathin Graphene-like Nanosheets as Stable Bifunctional Catalyst for Zn-Air Batteries. *Chemistry-an Asian Journal* **2021,** *16*, 1592–1602.
9. Battiato, S.; Urso, M.; Cosentino, S.; Pellegrino, A.L.; Mirabella, S.; Terrasi, A., Optimization of Oxygen Evolution Reaction with Electroless Deposited Ni-P Catalytic Nanocoating. *Nanomaterials (Basel)* **2021,** *11*, 11.
10. Zhang, L.; Mi, T.; Ziaee, M.A.; Liang, L.; Wang, R., Hollow POM@MOF hybrid-derived porous Co3O4/CoMoO4 nanocages for enhanced electrocatalytic water oxidation. *J. Mater. Chem. A* **2018,** *6*, 1639–1647.
11. Huang, Z.; Yang, Z.; Hussain, M.Z.; Chen, B.; Jia, Q.; Zhu, Y.; Xia, Y., Polyoxometallates@zeolitic-imidazolate-framework derived bimetallic tungsten-cobalt sulfide/porous carbon nanocomposites as efficient bifunctional electrocatalysts for hydrogen and oxygen evolution. *Electrochim. Acta* **2020,** *330*.
12. Zhang, J.-W.; Zhang, H.; Ren, T.-Z.; Yuan, Z.-Y.; Bandosz, T.J., FeNi doped porous carbon as an efficient catalyst for oxygen evolution reaction. *Frontiers of Chemical Science and Engineering* **2020,** *15*, 279–

287.
13. Tao, Z.; Wang, T.; Wang, X.; Zheng, J.; Li, X., MOF-Derived Noble Metal Free Catalysts for Electrochemical Water Splitting. *ACS Appl Mater. Interfaces* **2016,** *8*, 35390–35397.
14. Song, F.; Hu, X., Exfoliation of layered double hydroxides for enhanced oxygen evolution catalysis. *Nat. Commun* **2014**, *5*, 4477.
15. Xie, C.; Wang, Y.; Hu, K.; Tao, L.; Huang, X.; Huo, J.; Wang, S., In situ confined synthesis of molybdenum oxide decorated nickel–iron alloy nanosheets from MoO42− intercalated layered double hydroxides for the oxygen evolution reaction. *J. Mater. Chem. A* **2017,** *5*, 87–91.
16. Liu, Y.; Jiang, H.; Zhu, Y.; Yang, X.; Li, C., Transition metals (Fe, Co, and Ni) encapsulated in nitrogen-doped carbon nanotubes as bi-functional catalysts for oxygen electrode reactions. *J. Mater. Chem. A* **2016,** *4*, 1694–1701.
17. Zhang, X.; Xu, H.; Li, X.; Li, Y.; Yang, T.; Liang, Y., Facile Synthesis of Nickel–Iron/Nanocarbon Hybrids as Advanced Electrocatalysts for Efficient Water Splitting. *ACS Catal.* **2015,** *6*, 580–588.
18. Li, Y.; He, H.; Fu, W.; Mu, C.; Tang, X.Z.; Liu, Z.; Chi, D.; Hu, X., In-grown structure of NiFe mixed metal oxides and CNT hybrid catalysts for oxygen evolution reaction. *Chem Commun (Camb)* **2016,** *52*, 1439–1442.

.

.